Pages: 74-85 / Vol. 16/ Issue 2 / Summer- Fall 2023

Journal of Aerospace Science and Technology

www:jast.ias.ir

Scientific-Research Article

Numerical Study of Flattened Miniature Heat Pipe with Hybrid Porous Wick and Double Heat Sources

G.R. Abdizadeh[1] , **Sahar Noori**[2]***, Mohammad Saeedi**[3]**, Hamidreza Tajik**[4]

1-2- Department of Aerospace Engineering, Amirkabir University of Technology ,Tehran, Iran
3- Mechanical Engineering Department, Dalhousie University, Halifax,Canada
4- Satellite Research Institute, Tehran, Iran

ABSTRACT

Keywords: *Flattened heat pipe, hybrid wick, Thermal resistance, Numerical simulation*

Designing flattened miniature heat pipes (FMHPs) for electronic devices is challenging due to high heat flux and limited heat dissipation space. It requires understanding the combined effects of the sintered-grooved wick structure, double heat sources, and flat thickness on heat pipes' thermal efficiency. Therefore, this study aims to numerically investigate the effects of the FMHP with a hybrid wick on the thermal performance of its double heat sources acting as the CPU and GPU in notebook PCs. A transient 3D finite volume method solved the governing equations and assisted boundary conditions. The cylindrical heat pipe with a 200 mm length and 6 mm outside diameter is flattened into 2, 2.5, 3, and 4 mm final thicknesses (FT). The results show that the final critical thicknesses with the lowest thermal resistance are 2.5 and 3 mm for hybrid and grooved wick structures, respectively. Therefore, FMHP with hybrid wicks can be flattened about 8% more. Hybrid wick structures have the best effect on FMHP thermal performance at FT=2.5 mm.

Nomenclature

n	area (m^2)
A	
C_E	Ergun's coefficient, 0.03
h_{fg}	Latent heat (J/kg)
k	Thermal conductivity (W/m K)
k_{eff}	Effective thermal conductivity (W/m K)
K	Permeability (m^2)
L	Length of heat pipe (m)
$\dot{m}''$	Mass flux (kg/m^2s)
P	Pressure (Pa)
t	Time (s)
T	Temperature (K)
$\vec{V}$	Velocity vector (m/s)

Greek

σ	Accommodation coefficient
ρ	Density of liquid (kg/m^3)
ε	Porosity of the wick
μ	Dynamic viscosity (N s/m^2)

Subscripts

a	Adiabatic section
c	Condenser
e	Evaporator
eff	Effective
i	Interface
l	Liquid

1 PhD. Candidate
2 Associate Professor (Corresponding Author) Email: * s_noori@aut.ac.ir
3 Assistant Professor
4 PhD. Candidate

10.22034/jast.2023.400610.1154

Submit: 05.06. 2023/ Accepted: 18.07.2023
Print ISSN:2345-3648 Online ISSN: 1735-2134

s Solid
v Vapor
w Wick

Introduction

A miniature heat pipe (MHP) is a compact and efficient device that transfers heat from one point to another. A sealed cylindrical tube contains a working fluid, typically a low-boiling-point liquid such as water or a refrigerant. The heat pipe utilizes the principles of phase change and capillary action to transfer heat effectively [1, 2]. The basic construction of an MHP consists of an outer cylindrical shell made of a thermally conductive material, such as copper or aluminum. Inside the shell, there is a wick structure lining the inner surface. The wick is usually made of a porous material like sintered or woven metal mesh. The wick helps to facilitate the circulation of the working fluid within the heat pipe. Heat is applied to the wick at one end of the heat pipe, known as the evaporator section. This causes the working fluid to vaporize and form a vapor phase. The vapor moves towards the cooler end of the heat pipe, known as the condenser section, where it condenses into a liquid phase, releasing the absorbed heat. The condensed liquid then flows back to the evaporator section through the wick due to capillary action, completing the cycle [3-5].

The MHP is designed to be compact and suitable for applications with limited space or where weight is a concern. They are commonly used in various electronic devices, including laptops, smartphones, and other portable electronics, to efficiently transfer heat away from heat-generating components to heat sinks or other cooling mechanisms. The small size of the heat pipe allows for efficient heat transfer over relatively short distances, making it an ideal solution for localized cooling requirements. However, it's important to note that the specific design and dimensions of an MHP may vary depending on the application and desired heat transfer characteristics [1, 2].

Cylindrical heat pipes are usually flattened to fabricate flattened miniature heat pipes (FMHPs) due to the fabrication process being very efficient and low-cost. The wick is the most critical part of the heat pipe that provides sufficient capillary force and permeability for the working fluid to circulation. The performance and efficiency of the heat pipe are also a function of the wick's effective thermal conductivity, capillary pressure, and permeability coefficient [2]. The homogeneous and hybrid wicks are the two most common wick structures utilized within the heat pipes. Each homogeneous wick structure has different thermal characteristics. For example, the grooved wick has high permeability and low capillary pressure, and sintered powder wick has a low permeability coefficient and higher capillary pressure [6]. However, providing high permeability and high capillary force from a homogenous wick structure is challenging. To achieve these important features, studying the hybrid wick structures is essential. The sintered-grooved wick, a hybrid wick, has been developed to provide high permeability and capillary pressure [7]. Therefore, using a hybrid wick can improve the hydraulic efficiency of heat pipes.

Zhou et al. [8] fabricated an ultra-thin flattened heat pipe (UTFHP) with a thickness of 1.1 mm and a hybrid spiral-weaved mesh wick structure. The effect of the hybrid wick structures' layer number and pore size on the UTFHP's thermal performance was experimentally investigated. The results showed that thermal resistance decreased by 27.53–42.92%, using the suitable hybrid wicks. Abdizadeh et al. [9] numerically studied the thermal performance of thin flat heat pipes (TFHP) with mesh-grooved (hybrid) and grooved wicks for different heat inputs. The results indicated that for heat fluxes of 10, 20, and 30 W, the performance of TFHP with hybrid wick compared to grooved wick is improved by 3.59%, 20.38%, and 28.57%, respectively. It can be found that the hybrid wick plays an important role in improving the thermal performance of TFHP. Sudhakar et al. [10] designed a vapor chamber with a two-layer sintered porous evaporator wick. The two-layer wick design provides low thermal resistance and high heat dissipation. Li et al. [11], Naemsai et al. [12], and Deng et al. [13] investigated the effect of hybrid sintered-grooved and mesh-grooved wicks on the thermal performance of UTHPs.

Most literature studied the thermal characteristics of FMHPs with a single heat source and heat sink due to their simplicity. However, FMHP devices with multiple heat sources have been studied both experimentally and numerically. The effect of multi-heat sources on the thermal performance of the heat pipe with screen wick was studied by Faghri and Buchko [14]. They reported that the evaporators near the condenser section had more heat fluxes without affecting the operation of the farther evaporators. However, the heat flux capacity of the evaporator furthest from the condenser is reduced by adding more evaporators to the heat pipe. Shabgard and Faghri [15] developed analytical methods for a cylindrical heat pipe with multi-heat sources to predict vapor velocity and wall temperature in a steady-state condition. Using an analytical model, Subedi et al. [16] studied the thermal performance of flat-micro heat pipes with multiple heat sources and sinks. The effect of thickness, mesh wick diameter, and fiber separation distance on the maximum heat transfer rate of the FMHPs were investigated for capillary and maximum temperature limits.

Due to the geometrical limitations of the structure, the heat pipe is flattened to fit the narrow space. In addition, the contact area between a heat pipe and a processor chip can be increased with flattened heat pipes. The effect of flattening on the thermal characteristics of heat pipe has been investigated by several researchers [17-19]. It was found that thermal resistance increases with flattening and final thickness decreases. The flattening effect on the thermal performance of axially grooved heat pipe with a diameter of 6 mm was investigated by Tao et al. [17]. Their results indicated that the thermal resistance was enhanced from 0.1 to 0.4 when the overall thickness reduced from 6 to 2 mm. Intagun et al. [18] investigated the flattening effect on the performance of a sintered powder wick heat pipe by using a 3D finite element model. Their results showed that the total thermal resistance dropped from 0.91 to 0.88°C/W when the final thickness reduced from 4.0 to 2.5 mm. Sangpab et al. [19] experimentally studied a miniature heat pipe (MHP) with a sintered wick. Their study examined the combined effects of flattening and bending on the thermal performance of MHP. As a result of flattening and bending together, thermal resistance increased from 0.88 to 1.56 K/W (6 mm, 0° to 3 mm, 90°). However, these effects depend on the thickness of the MHP.

Based on the reviewed research, it has been found that the type of wick structure, multi-heat sources, and flat thickness affect the heat transfer characteristics of FMHPs. However, published literature has been focused on one effect at a time [3-19]. Designing FMHPs for electronic devices is challenging due to high heat flux and limited heat dissipation space. It requires understanding the combined effects of the hybrid wick, double heat sources, and flat thickness on heat pipes' thermal efficiency. In this regard, this work aims to numerically investigate the effects of the FMHP with a hybrid wick on the thermal performance of its double heat sources acting as the CPU and GPU in notebook PCs.

Model Description

The heat pipe consists of three main sections: evaporator, adiabatic, and condenser. As heat is applied to the evaporator section, the working fluid in the saturated liquid state is vaporized. The vapor pressure is increased in the evaporator section, so the hot vapor flows toward the lower-temperature condenser section. In the condenser section, the hot vapor condenses and releases heat. Finally, the condensation fluid is pumped back into the evaporator through the wick structure. Figure 1 depicts the schematic for the flattened and cylindrical heat pipes. The geometric specifications of the cylindrical heat pipe and other thermal properties were selected to conform to Naemsai et al. [12]. The cylindrical heat pipe with a 200 mm length and 6 mm outside diameter is flattened into 2, 2.5, 3, and 4 mm final thicknesses. In addition, it includes double heat sources with 15 mm length each, such as the CPU and GPU. Table 1 contains more information about geometry. The finite volume method (FVM) discretizes the presented model's governing equations into algebraic equations. The following diagram depicts the governing equations, boundary conditions, and numerical simulation.

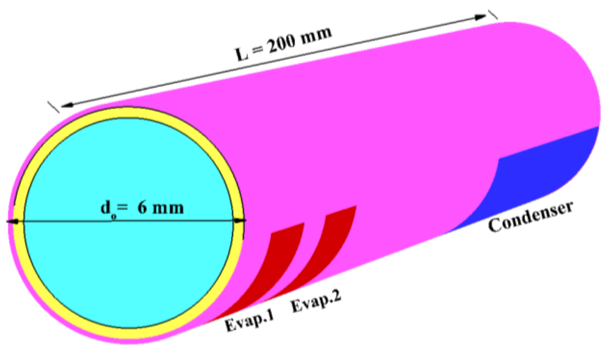

a) Cylindrical heat pipe.

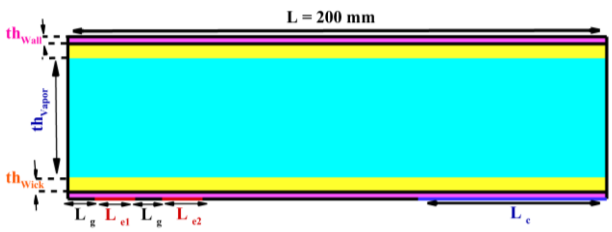

(b) Front view.

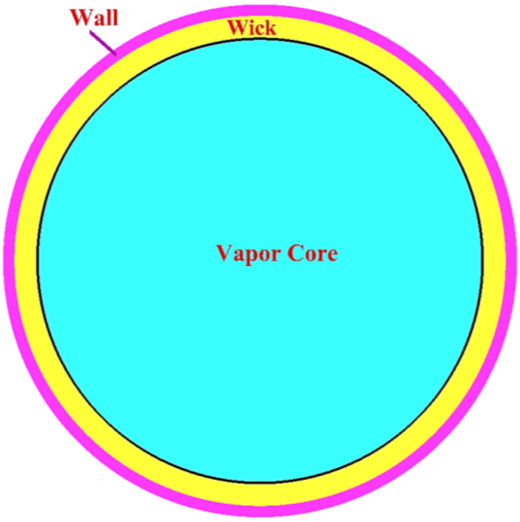

(c) Side view of cylindrical HP

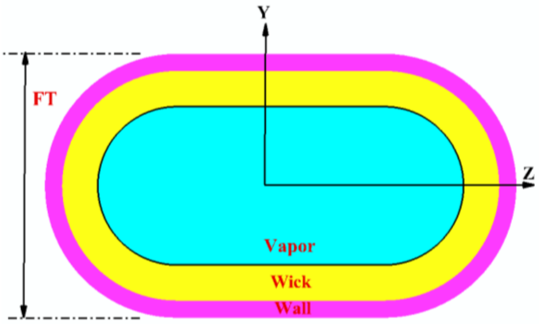

d) Side view of FMHP

Figure 1. Schematic of the cylindrical and FMHP.

Table 1. Detailed dimensions of the 3-D model.

Parameter		**Value (mm)**
Total length	L	200
Evaporator length	L_{e1}, L_{e2}	15
Distance from To evaporator 1	L_g	10
Condenser length	L_c	70
Outside diameter	d_o	6
Wall thickness	th_{wall}	0.26
Wick thickness	th_{wick}	0.54
Vapor core thickness	th_{vapor}	4.4
Flattened thickness	FT	2, 2.5, 3 and 4

Numerical Model

As shown in Figure 1, the geometric model consists of three computational domains: wall, grooved-sintered wick, and vapor core. They are separately solved and then linked together using boundary conditions at their interfaces. Fluid flow and heat transfer are solved using FVM for cylindrical and flattened miniature heat pipes. The formulation of continuity, Navier-Stokes, and energy equations is based on the following assumptions:

- A transient three-dimensional model is developed for heat transfer, mass transfer, and fluid flow.
- The fluid flows of the wick and vapor core are considered to be incompressible, laminar, and at saturation conditions.
- The hybrid wick and wall region thermo-physical properties are constant.
- Heat transfer in the wick region is modeled using an equilibrium model and an extended Brinkman-Forchheimer Darcy model.
- Using the ideal gas state equation, the change in density in the vapor is calculated.
- As the heat pipe operates horizontally, the effect of gravity is ignored.

Governing Equations

Transient and conservative forms of the governing equations are presented. For both the wick and vapor core, the continuity equation is as follows [19]:

$$\varepsilon\frac{\partial\rho}{\partial t}+\nabla.\left(\rho\vec{V}\right)=0 \qquad (1)$$

The $\frac{\partial\rho}{\partial t}$ describes mass addition and depletion within the vapor and wick domain, respectively. Note that the porosity for the vapor domain is $\varepsilon=1$. The Darcian transport equation calculates the kinetic energy of fluid within the wick domain. The unsteady 3D momentum equations in the wick and vapor domains are written as follows [19]:

$$\frac{\partial(\rho u)}{\partial t}+\nabla.\left(\rho\vec{V}u\right)=-\frac{\partial(\varepsilon P)}{\partial x}+\nabla.(\mu\nabla u)-\frac{\mu\varepsilon}{K}u-\frac{C_E\varepsilon}{K^{0.5}}\rho\left|\vec{V}\right|u \qquad (2)$$

$$\frac{\partial(\rho v)}{\partial t}+\nabla.\left(\rho\vec{V}v\right)=-\frac{\partial(\varepsilon P)}{\partial y}+\nabla.(\mu\nabla v)-\frac{\mu\varepsilon}{K}v-\frac{C_E\varepsilon}{K^{0.5}}\rho\left|\vec{V}\right|v \qquad (3)$$

$$\frac{\partial(\rho w)}{\partial t}+\nabla.\left(\rho\vec{V}w\right)=-\frac{\partial(\varepsilon P)}{\partial z}+\nabla.(\mu\nabla w)-\frac{\mu\varepsilon}{K}w-\frac{C_E\varepsilon}{K^{0.5}}\rho\left|\vec{V}\right|w \qquad (4)$$

The permeability (K) and Ergun coefficient of the porous media (C_E) are calculated by Ref.s [20, 21]. In the vapor core, permeability is K =∞. The energy equations for the wall, wick, and vapor core are written in equations (5) to (7), respectively. The subscripts s, l, and v denote solid, liquid, and vapor characteristics, respectively. The wick's effective thermal conductivity (k_{eff}) is determined by the solid and liquid conductivity and the type of wick structure used. k_{eff} is calculated using the correlation given by Ref.s [22, 23].

$$\text{For grooved wick: } k_{eff} = \frac{k_l(k_l + k_s - (1-\varepsilon)(k_l - k_s))}{k_l + k_s + (1-\varepsilon)(k_l - k_s)} \tag{8}$$

$$\text{For Sintered wick: } k_{eff} = \varepsilon . k_l + (1-\varepsilon)k_s \tag{9}$$

Table 2 shows the sintered-grooved wick expressions.
For a screen wick structure, the porosity and permeability can be estimated by [30]:

Table 2. Expressions for the sintered-grooved wick in governing equations.

Parameter	Sintered wick	Grooved wick
Ergun coefficient of the wick	$C_E = \alpha\beta^{-0.5}\varepsilon^{-1.5}, \alpha = 1.75, \beta = 150$ [20,21]	
Permeability	$K_{sw} = \frac{d^2\varepsilon^3}{150(1-\varepsilon)^2}$[24]	$K_{gw} = \frac{{D_{h,p}}^2\varepsilon}{2fRe_{h,p}}$[25]

Boundary conditions

This section describes the boundary conditions for the computational domain.
1.Wick-wall interface: The no-slip boundary condition and the energy balance at the interface are being used as follows:

$$V_l = 0 \tag{10}$$

$$k_s \left[\frac{\partial T}{\partial n}\right]_{wall} = k_{eff}\left[\frac{\partial T}{\partial n}\right]_{wick} \tag{11}$$

2. Wick-vapor interface: It is assumed that the phase change from liquid to vapor occurs at the wick-vapor interface. The interface temperature Ti is obtained from the energy balance at the interface.

$$-k_{eff}A_i\left[\frac{\partial T}{\partial y}\right]_{wick} = -k_v A_i\left[\frac{\partial T}{\partial y}\right]_{vapor} + m_i h_{fg} \tag{12}$$

The pressure at the interface P_i is calculated based on the Clausius-Clapeyron equation, with P_0 and T_0 being reference values:

$$\frac{R}{h_{fg}}\ln\left(\frac{P_i}{P_0}\right) = \frac{1}{T_0} - \frac{1}{T_i} \tag{13}$$

Based on the kinetic energy theory [26], the mass flux at the wick-vapor interface is calculated as follows:

$$\dot{m}_i'' = \left(\frac{2\sigma}{2-\sigma}\right)\frac{1}{\sqrt{2\pi R}}\left(\frac{P_v}{\sqrt{T_v}} - \frac{P_i}{\sqrt{T_i}}\right) \tag{14}$$

The accommodation coefficient σ is set to 0.03 in this study [26, 27].
3.Hybrid wick interface: The following energy balance is applied at the grooved-sintered wick interface.

$$k_{eff}\left[\frac{\partial T}{\partial n}\right]_{grooved} = k_{eff}\left[\frac{\partial T}{\partial n}\right]_{sintered} \tag{15}$$

4. Evaporator and condenser sections: The boundary conditions for evaporation and condensation sections are listed below.

$$\text{Evaperators: } -k\frac{\partial T}{\partial n} = \frac{Q_e}{A_e} \tag{16}$$

$$\text{Condenser: } -k\frac{\partial T}{\partial n} = -\frac{Q_{e1} + Q_{e2}}{A_c} \tag{17}$$

5. Adiabatic section and lateral wall: In the lateral wall and adiabatic section, velocity components, and temperature gradients are zero, based on the insulation and non-slip conditions applied as follows:

$$V = \left[\frac{\partial T}{\partial n}\right]_{wall} = 0 \tag{18}$$

Moreover, the initial conditions are imposed as follows:

$$T = T_\infty, P_{op}(t = 0) = P_{sat}\,(T_\infty) \tag{19}$$

6. Calculation of operating pressure in vapor core: The Pop is a function of time and is computed from the overall mass balance at the wick–vapor interface as follows [28]:

$$P_{op} = \frac{M_v^0 + \Delta t(\sum_{wick-vaper} - \dot{m}_t)}{\frac{1}{R}(\sum_{vaper-calls} \frac{V_{cell}}{T_v})} \tag{20}$$

Numerical procedure

The material of the wall and wick is copper, and the working fluid is water. The hybrid wick (sintered-grooved) was developed using a combination of spherical copper powders with a mean diameter of 220 µm and 55 µm axial grooves on the inside radius of the copper container [12]. The thermophysical properties of the wall, wick, and vapor core are presented in Table 3.

Table 3. Detailed thermophysical properties of domains.

Domain	Parameter	Value	Unit
Wall	Thermal conductivity	387.6	W/m.K
	Density	8978	Kg/m^3
	Specific heat	381	J/kg.K
Wick	Effective thermal conductivity of sintered wick	6.81	W/m.K
	Effective thermal conductivity of grooved wick	2.15	W/m.K
	Porosity	0.55	-
	Permeability of sintered wick	$1.23*10^{-10}$	m^2
	Permeability of grooved wick	$3.98*10^{-9}$	m^2
	Specific heat	4200	J/kg.K
Vapor	Thermal conductivity	0.0189	W/m.K
	Viscosity	$8.4*10^{-6}$	$N.s/m^3$
	Specific heat	1861	J/kg.K
Phase change	Latent heat	$2.473*10^6$	J/kg
Evaporator	Heat load	0:40	W

A 3D fully-implicit FVM is used to solve the governing equations and assisted boundary conditions in transient form. The diffusion and convective terms are discretized based on central difference and second-order upwind methods. The semi-implicit method is used the pressure and velocity coupling for the pressure-linked equations (SIMPLE) algorithm. An iterative algorithm guessed an initial pressure, then momentum equations were solved. Afterward, a pressure equation for pressure correction was utilized to satisfy the continuity equation. Iterations are completed when all scaled residuals become less than 10^{-6}. It is noted that the analysis was carried out on a computer with Intel® Xenon® CPU E5-2699 v3@ 2.3GHz and 32 GB RAM.

Grid independence study

In this section, the mesh dependence study was performed using five different grids to eliminate the effect of mesh resolutions on the computational results. The thermal resistances, evaporator temperature, and condenser temperature for various grids are compared in Table 4. As observed, the results for the number of cells 1.4×10^6 and 9.38×10^5 are almost the same value. Considering the grid with 6.25×10 to the fifth cells and 9.38×10 to the fifth cells, the thermal resistances, evaporator and condenser temperatures slightly change approximately 0.5%. Thus, the grid with 625,000 cells is selected for this study. Figure 2 illustrates the generated O-type structured grid (tetrahedral mesh) for the 3D computational domain.

Table 4. Grid independency.

Number of cells	T_e(°C)	T_c(°C)	Thermal resistances	Error (%)
$\mathbf{2.78 \times 10^5}$	67.24	51.41	0.395	9.7
$\mathbf{4.17 \times 10^5}$	70.67	54.13	0.413	5.6
$\mathbf{6.25 \times 10^5}$	72.35	54.9	0.436	0.5
$\mathbf{9.38 \times 10^5}$	72.5	55.01	0.4375	0
$\mathbf{1.4 \times 10^6}$	72.51	55.01	0.4375	0

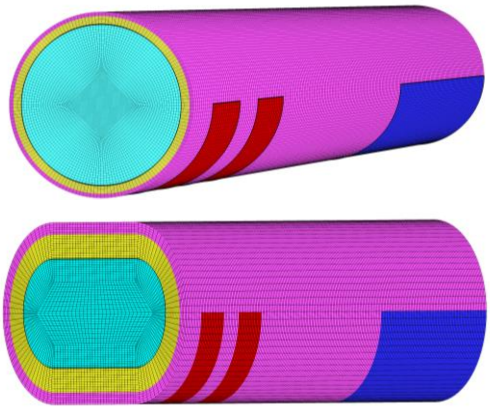

Figure 2. Computational grids for cylindrical and flattened miniature heat pipe.

Solver Validation

The results were compared to the experimental data provided by Zeghari et al. [29] to validate the numerical simulation presented in this paper. Table 5 shows the numerical data required for model implementation. The wall temperature distribution is compared in Figure 3 between the experimental results and the current numerical study. The results are consistent with the experimental data reported in Ref. [29]. The maximum temperature difference between the present work and Ref. [29] equals 1.6℃. In addition, Table 6 provides the thermal resistance obtained from the experimental results of Zeghari et al. compared to the results obtained from the presented numerical simulation in three different heat loads. The thermal resistances are accurately predicted with a maximum deviation of 6.97% from the experimental results.

Table 5. Parameters of the model implementation [29].

Parameter	Value	Unit
Working fluid	N-pentane	-
Wall and wick materia1	Copper	-
Heat input	7	W
Total length	225	mm
Evaporator length	30	mm
Condenser length	95	mm
Adiabatic length	100	mm
Outside diameter	4.5	mm
Wick structure	Sintered	-
Porosity	0.35	-
permeability	1.93×10^{-10}	m^2
effective thermal conductivity	1.47	W/m.K

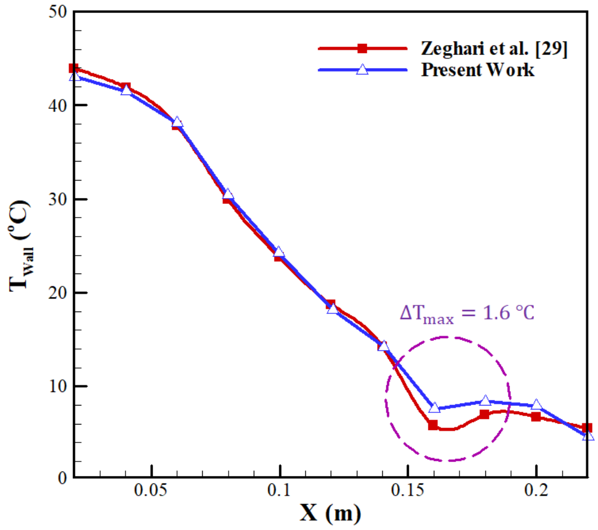

Figure 3. Comparison of experimental wall temperature with present numerical simulation.

Table 6. Comparison of experimental thermal resistance with present numerical simulation.

Heat input (W)	Thermal resistance (K/W)		Error (%)
	Zeghari et al. [29]	Present work	
5	5.45	5.07	6.97
7	4.73	4.45	5.9
12	4.22	4.01	5

Results and Discussion

The combined effects of flattening, grooved-sintered wick, and double heat source are studied on heat transfer performance FMHP. The velocity, vapor pressure, temperature, and thermal resistance parameters are presented for various input heat loads. The evaporators closest to the condenser section is carried greater heat loads without affecting the performance of the evaporators farther away. Adding additional heat to evaporators further away from the condenser, on the other hand, may reduce the heat pipe's maximum heat transfer limit [14]. Therefore, the present work applies more heat load to the evaporator near the condenser. The applied total heat load to evaporators 1 and 2 is 40 W (evaporator 1: evaporator 2; 0:40, 10:30, and 20:20 W).

Effect of double heat source and flatting in sintered-grooved wick

The distribution of vapor velocity and vapor pressure along the axial length of FMHP for various flattened thicknesses and heat inputs are illustrated in Figures 4 and 5, respectively. The vapor velocity increases with a decrease in the final thickness, and the vapor core becomes thinner at the same heat loads. For instance, in a heat load of 0:40 W, as the final thickness decreases from 6 to 2.5 mm, the maximum value of vapor velocity gradually increases from 13.39 to 34.57 m/s. Still, when the final thickness reduces from 2.5 to 2 mm, the maximum value of vapor velocity sharply increases about two times (Figure 4). A similar trend is observed for the results of vapor pressure. As shown in Figure 5, the vapor pressure difference increases significantly due to the narrow vapor core when the final thickness reduces from 2.5 to 2 mm.

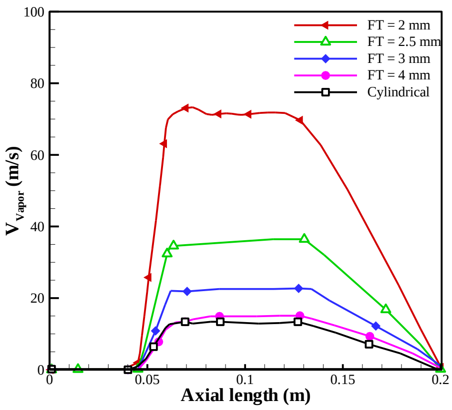

(a) Heat input 0:40 W.

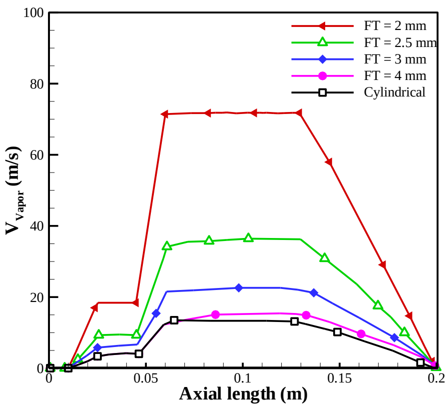

(b) Heat input 10:30 W.

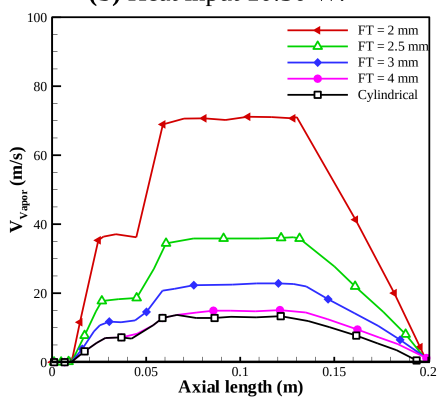

(c) Heat input 20:20 W.

Figure 4. Vapor velocity at the center of the vapor core.

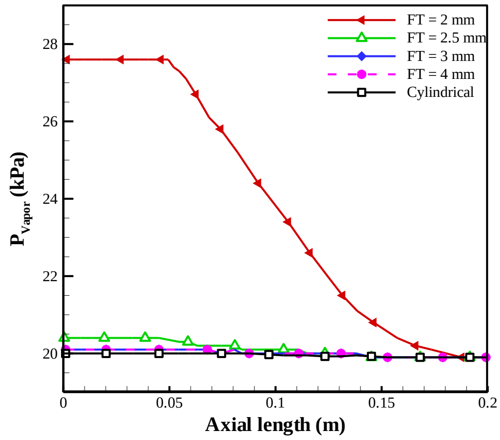

(a) Heat input 0:40 W.

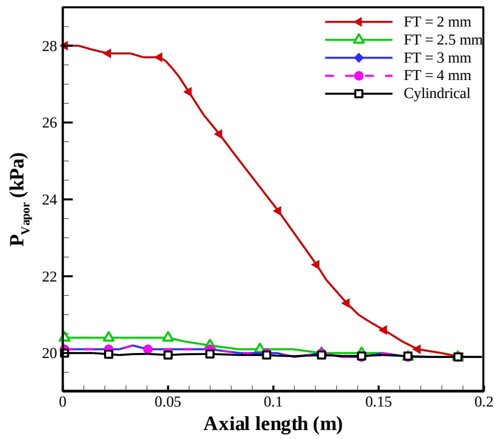

(b) Heat input 10:30 W.

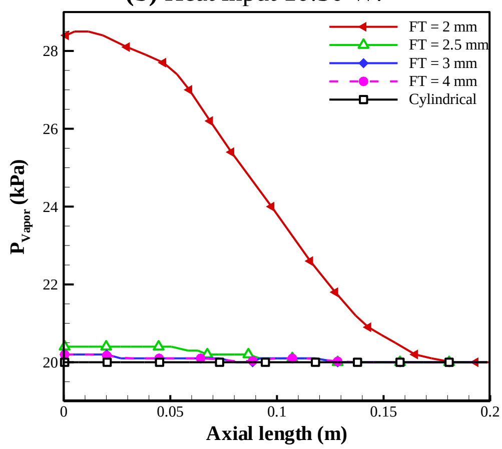

(c) Heat input 20:20 W.

Figure 5. Vapor pressure at the center of the vapor core.

Figure 6 illustrates the wall temperature distribution of FMHP with FT= 4.0 and 2.5 mm in different heat inputs. The temperature is higher during the evaporator sections because they are set on a heating source. Then, it decreases during the adiabatic zone and remains constant until the condenser section, where heat is removed from the ambiance through forced convection, resulting in significant temperature drops. By decreasing FT from 4 to 2.5 mm, wall temperatures are dropped by about 5% because the contact surface increases by 12%. Also, the maximum value of wall temperature in heat loads of 0:40, 10:30, and 20:20 W decreased by 4.4, 3.99, and 3.45%, respectively. On the other hand, the contacted surface of FMHP with FT=2 mm was larger, but the pressure drop sharply increased due to the narrower vapor core. Thus, the maximum value of the wall temperature for FMHP with FT=2 mm equals 96°C. However, with temperatures below 100 ° C, the CPU, and GPU perform efficiently [1]. As a result, the wall temperature difference grew dramatically if the final thickness surpassed the specific value. It is noted that the particular value in this research is 2.5 mm.

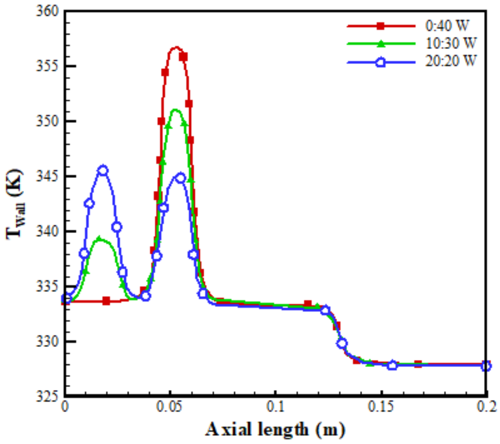

(a) Final thickness of 4 mm.

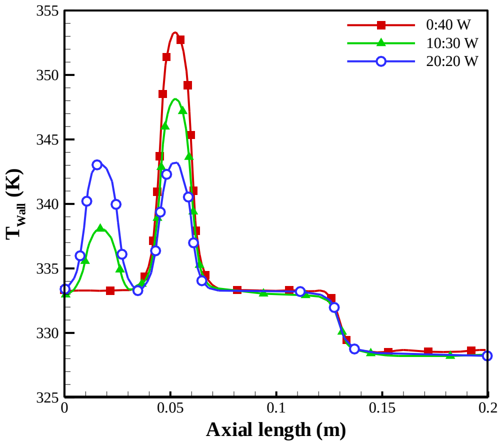

(b) Final thickness of 2.5 mm.

Figure 6. Wall temperature distribution of FMHP.

Thermal resistance is used to assess the efficiency of the cooling device. As demonstrated in Eq. (21), thermal resistance is defined as the difference between the temperature of the condenser and evaporator sections divided by the heat loads.

$$R_{th} = \frac{\overline{T}_e - \overline{T}_c}{Q_{e1} + Q_{e2}} \tag{21}$$

It was reported that the heat pipe with lower thermal resistance efficiently transfers heat [2]. Figure 7 illustrates the effect of different final thicknesses on the thermal resistance of heat pipes at various heat loads. The results indicated that as FT decreases from 4 to 2.5 mm, R_{th} is reduced from 0.525 to 0.437 K/W due to enhancement in the contacted surface, leading to the reduction in heat flux at evaporators 1 and 2. If FMHP is flattened to 2 mm, the R_{th} is enhanced to 0.6 K/W, decreasing thermal performance. The final critical thickness with the lowest thermal resistance is 2.5 mm. As shown in Fig. 7, the thermal resistance value is approximately the same for different heat loads at FT= 2.5 mm.

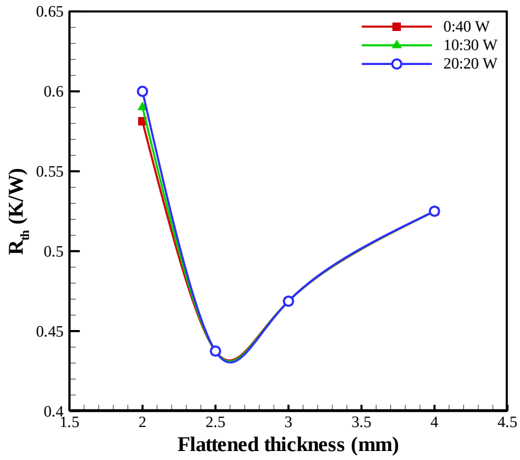

Figure 7. The thermal resistance of heat pipe versus different final thicknesses.

Effect of the type of wick structure on the thermal performance of FMHP

The thermal resistances of FMHPs with hybrid (sintered-grooved) and grooved wick structures are depicted in Figure 8 for different heat inputs. The final critical thicknesses with the lowest thermal resistance are 2.5 and 3 mm for hybrid and grooved wick structures, respectively. Therefore, FMHP with hybrid wicks can be flattened about 8% more. For FT<3 mm, by increasing the heat load of the evaporator farther away from the condenser section, the thermal resistance of the FMHP with grooved wick decreases. But, for FT>=3, the thermal performance of FMHP with the grooved wick increases if more heat load is applied at the evaporator closer to the condenser section. It can also be found that the variations of thermal resistance in different heat loads are not noticeable for the hybrid wick.

For heat input of 20:20 and 0:40 W, the performance of the FMHP with grooved wick compared to hybrid wick at FT= 2 and 4 mm is improved by 1.3% and 2.85%, respectively. In other cases, the thermal performance of FMHP with the hybrid wick is better. As observed in Figure 8, the most excellent effect of the hybrid wick structure on the thermal performance of FMHP is related to FT=2.5 mm. For heat loads of 0:40, 10:30, and 20:20 W at FT=2.5mm, the thermal performance of FMHP is improved by 23%, 16.75%, and 13.5%, respectively. Thus, the thermal performance improvement of FMHP with the hybrid wick is more significant.

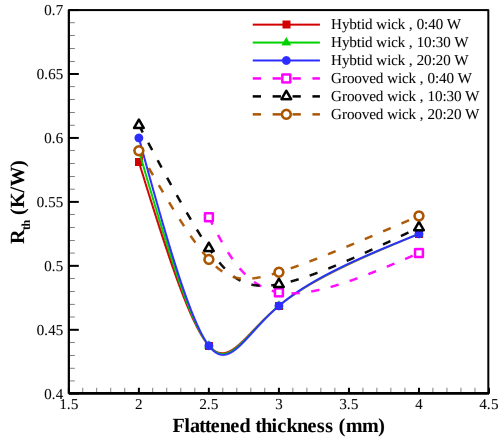

Figure 8. Effect of wick structures on the thermal resistances of FMHP

Conclusions

A transient 3D FVM solved the governing equations and assisted boundary conditions. The combined effects of the hybrid wick, multi heat sources, and flat thickness on the thermal performance of FMHP were investigated. The following findings are listed from the present study:

- The vapor velocity increases with a decrease in the final thickness, and the vapor core becomes thinner at the same heat loads. A similar trend is observed for the results of vapor pressure.
- The wall temperature difference grew dramatically if the final thickness surpassed 2.5 mm.
- As FT decreases from 4 to 2.5 mm, Rth is reduced from 0.525 to 0.437 K/W, and for FT=2mm increases Rth to 0.6 K/W.
- The final critical thicknesses with the lowest thermal resistance are 2.5 and 3 mm for hybrid and grooved wick structures, respectively. Therefore, FMHP with hybrid wicks can be flattened about 8% more.
- For FT<3 mm, by increasing the heat load of the evaporator farther away from the condenser section, the thermal resistance of the FMHP with grooved wick decreases.
- For FT≥3 mm, the thermal performance of FMHP with the grooved wick increases if more heat load is applied at the evaporator closer to the condenser section.
- For heat input of 20:20 and 0:40 W, the performance of the FMHP with grooved wick compared to hybrid wick at FT= 2 and 4 mm is improved by 1.3% and 2.85%, respectively. In other cases, the thermal performance of FMHP with the hybrid wick is better.
- Hybrid wick structures have the best effect on FMHP thermal performance at FT=2.5 mm.

References

[1] H. Tang, Y. Tang, Z. Wan, J. Li, W. Yuan, L. Lu, Y. Li, K. Tang, "Review of applications and developments of ultra-thin micro heat pipes for electronic cooling," Applied energy, vol. 223, pp. 383–400, Aug 2018.
[2] B. Zohuri, "Heat pipe design and technology: Modern applications for practical thermal management," Springer, 2016.
[3] T. Brahim, A. Jemni, "CFD analysis of hotspots copper metal foam flat heat pipe for electronic cooling applications," International Journal of Thermal Sciences, vol. 159, p. 106583, Jan 2021.
[4] H. Tang, C. Weng, Y. Tang, H. Li, T. Xu, T. Fu, "Thermal performance enhancement of an ultra-thin flattened heat pipe with multiple wick structure," Applied Thermal Engineering, vol. 183, p. 116203, Jan 2021.
[5] S. Pouryoussefi, S. G. Pouryoussefi, "Numerical study of flow visualization and thermal performance for pulsating heat pipes," Journal of Aerospace Science and Technology, vol. 15(2), pp. 17-24, 2022. doi: 10.22034/jast.2022.346070.1119
[6] G. Wang, Z. Quan, Y. Zhao, H. Wang, "Performance of a flat-plate micro heat pipe at different filling ratios and working fluids," Applied Thermal Engineering, vol. 146, pp. 459–468, 2019.
[7] L. Jiang, J. Ling, L. Jiang, Y. Tang, Y. Li, W. Zhou, J. Gao, "Thermal performance of a novel porous crack composite wick heat pipe," Energy Conversion and Management, vol. 81, pp. 10–18, 2014.
[8] W. Zhou, Y. Li, Z. Chen, L. Deng, B. Li, "Experimental study on the heat transfer performance of ultra-thin flattened heat pipe with hybrid spiral woven mesh wick structure," Applied Thermal Engineering, vol. 170, p. 115009, 2020.
[9] G. Abdizadeh, S. Noori, H. R. Tajik, M. Shahryari, M. Saeedi, "Numerical investigation of hybrid wick structure effect on thermal performance of a thin flat heat pipe," Amirkabir Journal of Mechanical Engineering, vol. 53, pp. 5485-5504, 2021.
[10] S. Sudhakar, J. A. Weibel, F. Zhou, E. M. Dede, S. V. Garimella, "Area-scalable high-heat-flux dissipation at low

thermal resistance using a capillary-fed two-layer evaporator wick," International Journal of Heat and Mass Transfer, vol. 135, pp. 1346–1356, 2019.
[11] Y. Li, W. Zhou, J. He, Y. Yan, B. Li, Z. Zeng, "Thermal performance of ultra-thin flattened heat pipes with composite wick structure," Applied Thermal Engineering, vol. 102, pp. 487–499, 2016.
[12] T. Naemsai, N. Kammuang-lue, P. Terdtoon, P. Sakulchangsatjatai, "Numerical model of heat transfer characteristics for sintered-grooved wick heat pipes under non-uniform heat loads," Applied Thermal Engineering, vol. 148, pp. 886–896, 2019.
[13] D. Deng, Y. Tang, G. Huang, L. Lu, D. Yuan, "Characterization of capillary performance of composite wicks for two-phase heat transfer devices," International Journal of Heat and Mass Transfer, vol. 56, pp. 283–293, 2013.
[14] A. Faghri, M. Buchko, Experimental and numerical analysis of low temperature heat pipes with multiple heat sources, pp. 728-734, 1991.
[15] H. Shabgard, A. Faghri, "Performance characteristics of cylindrical heat pipes with multiple heat sources," Applied Thermal Engineering, vol. 31, pp. 3410–3419, 2011.
[16] B. Subedi, S. H. Kim, S. P. Jang, M. Kedzierski, "Effect of mesh wick geometry on the maximum heat transfer rate of flat-micro heat pipes with multi-heat sources and sinks," International journal of heat and mass transfer, vol. 131, pp. 537–545, 2019.
[17] H.-Z. Tao, H. Zhang, J. Zhuang, W. J. Bowman, "Experimental study of heat transfer performance in a flattened AGHP," Applied thermal engineering, vol. 28, pp. 1699–1710, 2008.
[18] W. Intagun, P. Terdtoon, P. Sakulchangsatjatai, "Flattening effect on heat transfer characteristics of a sintered-wick heat pipe," American Journal of Applied Sciences, vol. 10, pp. 760–766, 2013.
[19] N. Sangpab, N. Kimura, P. Terdtoon, P. Sakulchangsatjatai, N. Kammuang-lue, M. Murakami, "Combined effect of bending and flattening on heat transfer performance of cryogenic sintered-wick heat pipe," Applied Thermal Engineering, vol. 148, pp. 878–885, 2019.
[20] D. A. Nield, A. Bejan, et al., "Convection in porous media", vol. 3, Springer, 2006.
[21] G. Carbajal, C. Sobhan, G. Peterson, D. Queheillalt, H. Wadley, "Thermal response of a flat heat pipe sandwich structure to a localized heat flux," International Journal of Heat and Mass Transfer, vol. 49, pp. 4070–4081, 2006.
[22] C. Li, G. Peterson, "The effective thermal conductivity of wire screen," International Journal of Heat and Mass Transfer, vol. 49, pp. 4095–4105, 2006.
[23] B. Xiao, A. Faghri, "A three-dimensional thermal-fluid analysis of flat heat pipes," International Journal of Heat and Mass Transfer, vol. 51, pp0 3113–3126, 2008.
[24] N. Pooyoo, S. Kumar, J. Charoensuk, A. Suksangpanomrung, "Numerical simulation of cylindrical heat pipe considering non-darcian transport for liquid flow inside wick and mass flow rate at liquid–vapor interface," International journal of heat and mass transfer, vol. 70, pp. 965–978, Mar 2014.
[25] S. J. Kim, J. K. Seo, K. H. Do, "Analytical and experimental investigation on the operational characteristics and the thermal optimization of a miniature heat pipe with a grooved wick structure," International Journal of Heat and Mass Transfer, vol. 46, pp. 2051–2063, May 2003.
[26] V. Carey, "Liquid-Vapor Phase-Change Phenomena: An Introduction to the Thermophysics of Vaporization & Condensation in Heat Transfer Equipment," Taylor & Francis, 2020.
[27] M. Famouri, G. Carbajal, C. Li, "Transient analysis of heat transfer and fluid flow in a polymer-based micro flat heat pipe with hybrid wicks," International Journal of Heat and Mass Transfer, vol. 70, pp. 545–555, Mar 2014.
[28] S. V. Patankar, "Numerical heat transfer and fluid flow," CRC press, 2018.
[29] K. Zeghari, H. Louahlia, "Flat miniature heat pipe with sintered porous wick structure: experimental and mathematical Studies," International Journal of Heat and Mass Transfer, vol. 158, p. 120021, Sep 2020.